Radial deformation and band-gap modulation of pressurized carbon nanotubes

Hisao Taira[*1], Hiroyuki Shima[2], Yoshitaka Umeno[3] and Motohiro Sato[1]

[1]*Division of Engineering and Policy for Sustainable Environment, Faculty of Engineering, Hokkaido University, Kita 13 Nishi 8, Kita-ku, Sapporo 060-8628, Japan*
[2]*Department of Environmental Sciences & Interdisciplinary Graduate School of Medicine and Engineering, University of Yamanashi, 4-4-37, Takeda, Kofu, Yamanashi 400-8510, Japan*
[3]*Institute of Industrial Science, The University of Tokyo, 4-6-1 Komaba, Meguro-ku, Tokyo 153-8505, Japan*

Abstract. We numerically investigate the electronic band structure of carbon nanotubes (CNTs) under radial corrugation. Hydrostatic pressure application to CNTs leads to a circumferential wave-like deformation of their initially circular cross-sections, called radial corrugations. Tight-binding calculation was performed to determine the band gap energy as a function of the amplitude of the radial corrugation. We found that the band gap increased with increasing radial corrugation amplitude; then, the gap started to decline at a critical amplitude and finally vanished. This non-monotonic gap variation indicated the metal-semiconductor-metal transition of CNTs with increasing corrugation amplitude. Our results provide a better insight into the structure-property relation of CNTs, thus advancing the CNT-based device development.

Keywords: carbon nanotube; radial corrugation; electronic structure; band gap energy; numerical calculation

1. Introduction

Numerical band calculations based on the tight-binding method have accelerated our understandings of the relation between mechanical and electronic properties (Umeno *et al.* 2004a,b, Ren *et al.* 2009, Umeno 2011, Lu *et al.* 2011, Choudhary and Qureshi 2012, Wong *et al.* 2012, Azevedo *et al.* 2013). Semiconducting zigzag single-walled CNTs (SWCNTs) show a semiconductor-metal transition (SMT) under increasing radial compression (Nishidate and Hasegawa 2008). Experimental observation supports this behavior where compression is induced by the tip of an atomic force microscope (AFM) (Barboza *et al.* 2008). Axial tension in the metallic CNTs results in a metal-semiconductor-metal transition (MSMT). These transitions are based on the concept of the one-electron approximation. Effects of many-body interaction in CNTs under uniaxial deformation result in Peierls distortions (Chen *et al.* 2008, Poklonski *et al.* 2012)

---

[*]Corresponding author, Ph.D., JSPS Research Fellow, E-mail: taira@eng.hokudai.ac.jp

whereas the electrons in undeformed CNTs behave as a Tomonaga-Luttinger liquid (Ishii *et al.* 2003, Kanbara *et al.* 2004). These findings indicate that the mechanical deformation of CNTs is a key factor in their applications in nanoelectronic and nanoelectromechanical devices (Ke *et al.* 2006, Farshidianfar and Soltani 2012, Pantano *et al.* 2013).

There have been numerous investigations of the mechanical properties of both single- and multi-walled CNTs (SWCNTs and MWCNTs) (Shima and Sato 2008, Shima *et al.* 2010, Huang *et al.* 2011, Shima *et al.* 2012, Silvestre 2012, Silvestre *et al.* 2012, Faria *et al*. 2012, 2013). Hydrostatic pressure causes cross-sectional deformation, called radial corrugation, within the continuum mechanics. The radius of the cross section shrinks under pressure and varies its shape into the radially corrugated mode when the pressure exceeds a critical value. These behaviors also remind us that this change of cross-sectional geometry may provide a wide variety of electronic properties. However, no attention has been paid to the relation between electronic properties and radial corrugation.

In the present paper, we perform numerical band calculations of a zigzag SWCNT subjected to radial corrugation. Radially corrugated configurations of atoms are assumed by the application of an envelope function to the ideal CNT structure and the electron structure to be obtained by the tight-binding approximation. The band structure and the band gap energy are expressed as a function of the magnitude of radial corrugation.

2. Radial elastic deformation of CNTs

2.1 Radial stiffness estimation

Radial deformation of CNTs has been intensively studied in the last decade from both theoretical and experimental viewpoints (See references in Shima *et al.* 2012). In the seminal work by Lordi and Yao (1998), for instance, the mechanical force-structure relationship of CNTs under asymmetric radial compression was revealed by using molecular dynamics simulations. They concluded that the mechanical stiffness of the concentric walls is enhanced by increasing the tube diameter and the number of layers. Reich *et al*. (2002) conducted an *ab initio* calculation on the effective radial modulus of nanotubes with diameter of 0.8 nm under hydrostatic pressure, which gave a value of 650 GPa. Li and Chou (2003) studied the elastic deformation of single-walled nanotubes under hydrostatic pressure by using the molecular structural mechanics method, which was developed by linking the molecular mechanics constants of force fields and frame sectional stiffness parameters. The study showed that the effective radial Young's modulus (by viewing the tube as solid cylinder) is highly dependent on the tube diameter. It decreases rather rapidly with increasing tube diameter.

2.2 Existing experiments

Experimental attempts have been made to measure the radial deformation of CNTs using different testing techniques. Chesnokov *et al.* (1999) experimentally found that the radial deformation of SWNTs with a 1.36 nm- diameter is reversible up to 2.9 GPa. Later, it was observed that the radial deformation of a bundle of SWNTs with a diameter of 1.4 nm is reversible up to 4 GPa (Tang *et al*. 2000, 2002). However, in the case of MWCNTs, only one experimental result is available thus far (Tang *et al*. 2000). In that experiment, the electrical resistance and

capacitance of MWCNTs with 20 layers and an innermost diameter of 3 nm were measured under pressure. Only a slight change in the electrical structure of the nanotubes was observed that was induced by a high pressure of up to 1.4 GPa.

Shen *et al*. (2000) used a microscope method to investigate the radial compression of multi-walled nanotubes under an asymmetric stress. They observed that the radial compressive modulus increased from 9.7 to 80 GPa when a tube with a 10-nm diameter was compressed by an amount between 26% and 46% in diameter. Yu *et al*. (2000) studied the radial deformability of a MWCNT to observe that by treating the tube as a uniform and isotropic solid cylinder with a Poisson's ratio of 0.5, a tube with an outermost diameter of 8 nm had effective radial modulus values of 0.3 to 4 GPa at different measured sections, which are comparable to the Young's modulus values of semi-crystalline polymers.

2.3 Radial corrugation of MWCNTs

Unlike "asymmetric" compression, spatially "isotropic" compression by hydrostatic pressure provides an ideal condition to study the radial deformation of CNTs. Tang *et al*. (2000) investigated the compressibility and polygonization of SWCNT-bundles under hydrostatic pressure using a diamond anvil cell and *in situ* x-ray diffraction. The volume compressibility of a bundle with a lattice constant of 17.2 Å and a tube diameter of 14.1 Å was found to be 0.024 GPa^{-1}.

In contrast to the intensive studies on SWCNTs (and their bundles), radial deformation of MWCNTs remains relatively unexplored. The multilayered structure of MWNTs is intuitively expected to enhance radial stiffness compared to SWCNTs. However, when the number of concentric walls is much greater than unity, the outside walls have large diameters, so external pressure may lead to a mechanical instability in the outer walls. This local instability triggers a novel cross-sectional deformation, called radial corrugation, of MWCNTs under hydrostatic pressure. Such a radial corrugation phenomenon is peculiar to MWCNTs in which the number of constituent walls is much greater than unity. In a corrugation mode, only a few outermost walls show significant radial corrugation along the circumference, while the innermost tube maintains its cylindrical symmetry.

From an engineering perspective, the tunability of the cross-sectional geometry may be useful for developing nanotube-based nanofluidic or nanoelectrochemical devices because both utilize the hollow cavity within the innermost tube. Another interesting implication is a pressure-driven change in the quantum transport of π electrons moving along the radially deformed nanotube. Mobile electrons whose motion is confined to a two-dimensional curved thin layer are known to behave differently from those on a conventional flat plane because of an effective electromagnetic field that can affect low-energy excitations of the electrons (Shima *et al*. 2009). Associated variations in electron-phonon coupling (Ono and Shima 2009) and phononic transport through deformed nano-carbon materials are also interesting and relevant to the physics of radially corrugated MWNTs. This background motivated us to perform electronic energy-band calculation of corrugated MWNTs as the first-step toward versatile applications.

3. Model and method

3.1 Tight-binding hamiltonian

Herein, we perform a numerical band calculation based on the tight-binding method. We first express the on-site parameters by using the surrounding environment of each atom and parameterize the hopping and overlap matrix elements by the method of Mehl and Papaconstantopoulos (1996) and Papaconstantopoulos *et al.* (1998).

The total energy of itinerant electrons using density functional theory based on the Kohn-Sham equation is given by

$$E[n(\boldsymbol{r})] = \sum_i f(\mu = \varepsilon_i)\varepsilon_i + F[n(\boldsymbol{r})] \tag{1}$$

where $n(\boldsymbol{r})$ is the electronic density at the position indicated by the position vector $\boldsymbol{r}$, ε_i is the Kohn-Sham eigenenergy of the *i*th electronic eigenstate, μ is the chemical potential, the sum with respect to *i* is over all electronic eigenstates, and $f(\mu - \varepsilon_i)$ is the Fermi-Dirac distribution function. The functional *F[n(r)]* is expressed by

$$F[n(\boldsymbol{r})] = T[n(\boldsymbol{r})] + V[n(\boldsymbol{r})] + E_{ex}[n(\boldsymbol{r})] \tag{2}$$

where $T[n(\boldsymbol{r})]$ is the total kinetic energy of electrons without any interaction, $V[n(\boldsymbol{r})]$ is the classical Coulomb potential energy, and $E_{ex}[n(\boldsymbol{r})]$ is the exchange-correlation energy.

On-site terms are dependent on the environment of each atom. We can express this environment by defining a pseudo-atomic density for each atom as

$$\rho_i = \sum_j e^{-\lambda^2 |r_i - r_j|} f_c\left(\left|r_i - r_j\right|\right) \tag{3}$$

where r_i and r_j are the position of the *i*th and *j*th atoms, respectively. λ is a parameter depending on the atom types, ρ_i is obtained by summing the contributions from all nearest neighbor sites of atom *i*. $f_c\left(\left|r_i - r_j\right|\right)$ is a cutoff function (Mehl and Papaconstantopoulos1996) given as follows

$$f_c\left(\left|r_i - r_j\right|\right) = \frac{1}{1 + \exp\left[\dfrac{(\left|r_i - r_j\right|) - r_0}{R}\right]} \tag{4}$$

where r_0 and *R* have been set to $r_0 = 14.0a_0$ and $R = 0.5a_0$, respectively. a_0 is the Bohr radius, and the cut-off distance is assumed to be 6.0 a_0. On-site terms for atom *i* yield

$$h_{il} = \alpha_l + \beta_l \rho_i^{2/3} + \gamma_l \rho_i^{4/3} + \chi \rho_i^2 \tag{5}$$

where *l* denotes the orbital indexes *s* and *p*. This means that the on-site terms are determined by nine parameters: $\alpha_l, \beta_l, \gamma_l, \chi_l, \lambda$

Next, we focus on the hopping terms of the Hamiltonian. We assume that the hopping energy decreases exponentially as the atomic distance increases

$$H_{ll'\mu}\left(\left|r_i - r_j\right|\right) = \left[a_{ll'\mu} + b_{ll'\mu}\left|r_i - r_j\right| + c_{ll'\mu}\left|r_i - r_j\right|^2\right]\exp(-d_{ll'\mu}^2\left|r_i - r_j\right|)f_c\left(\left|r_i - r_j\right|\right) \tag{6}$$

It is natural that the overlap parameters also exponentially decrease as the same functional form of the hopping terms

Table 1 Slater-Koster tight-binding parameters for carbon. Ry is the Rydberg unit (after Papaconstantopoulos *et al.* 1998)

On-site parameters given in Eqs. (1) and (2)				
λ	1.59901905594			
Orbital	α (Ry)	β (Ry)	γ (Ry)	χ (Ry)
s	-0.102789972814	-0.162604640052	-178.884826119	4516.11342028
p	0.542619178314	2.73454062799	-67.139709883	438.52883145
Hopping Parameters given in Eq. (6)				
Orbital	a (Ry)	b (Ry/a_0)	c (Ry/ a_0^2)	d (a_0^{-2})
$H_{ss\sigma}$	74.0837449667	-18.3225697598	-12.5253007169	1.41100521808
$H_{sp\sigma}$	-7.9172955767	3.6163510241	1.0416715714	1.16878908431
$H_{pp\sigma}$	-5.7016933899	1.0450894823	1.5062731505	1.13627440135
$H_{ss\pi}$	24.9104111573	-5.0603652530	-3.6844386855	1.36548919302
Overlap Parameters given in Eq. (7)				
Orbital	p (a_0^{-1})	q (a_0^{-2})	r (a_0^{-3})	s ($a_0^{-1/2}$)
$S_{ss\sigma}$	0.18525064246	1.56010486948	-0.308751658739	1.13700564649
$S_{sp\sigma}$	1.85250642463	-2.50183774417	0.178540712033	1.12900344616
$S_{pp\sigma}$	-1.29666913067	0.28270660019	-0.022234235553	0.76177690688
$S_{ss\pi}$	0.74092406925	-0.07310263856	0.016694077196	1.02148246334

$$S_{ll'\mu}\left(\left|r_i - r_j\right|\right) = \left[\delta_{ll'} + p_{ll'\mu} + q_{ll'\mu}\left|r_i - r_j\right| + r_{ll'\mu}\left|r_i - r_j\right|^2\right] \times \exp\left(-s_{ll'\mu}^2\left|r_i - r_j\right|\right) f_c\left(\left|r_i - r_j\right|\right) \qquad (7)$$

where $\delta_{ll'}$ is Kronecker's delta. We need the four types of the Slater-Koster parameters $(ll'\mu) = (ss\sigma), (sp\sigma), (pp\sigma), (pp\pi)$, where σ and π show the electron's orbital, since we focus on s and p orbitals. Therefore, the hopping and overlap terms are determined by 16 parameters $a_{ll'\mu}, b_{ll'\mu}, c_{ll'\mu}, d_{ll'\mu}$ and $p_{ll'\mu}, q_{ll'\mu}, r_{ll'\mu}, s_{ll'\mu}$ respectively. In summarizing, to solve the eigenvalue problem, we need one parameter λ, 8 parameters $\alpha_l, \beta_l, \gamma_l, \chi_l$, 16 parameters $a_{ll'\mu}, b_{ll'\mu}, c_{ll'\mu}, d_{ll'\mu}$ and $p_{ll'\mu}, q_{ll'\mu}, r_{ll'\mu}, s_{ll'\mu}$.

To obtain parameters, we shift the eigenvalues by a constant C, which is dependent on the lattice structure S and volume V. The resulting total energy is given by

$$E(S,V) = \sum_i \left[\varepsilon_i + C(S,V)\right] = \sum_i \varepsilon_i' \qquad (8)$$

where

$$C(S,V) = \frac{F\left[n(r)\right]}{N} \qquad (9)$$

and

$$N = \sum_i f(\mu' - \varepsilon_i') \tag{10}$$

with

$$\mu' = \mu + C(S,V) \tag{11}$$

Here, the sum in Eq. (10) is performed over all contributions from occupied electron states, and thus N equals to the number of electrons in the system. The tight-binding parameters are set to reproduce both the total energy and shifted energy without any basic proposition or assumption. We used the parameters obtained by Papaconstantopoulos *et al.* (1998) for carbon, which are given in Table 1.

3.2 Corrugation mode assumption

We evaluate (1) the electronic band gap energy, and (2) the electronic band structure, as changing in the corrugation amplitude under radial corrugation. In this work, we demonstrate the cases of metallic and semiconducting zigzag SWCNTs whose chiral vectors are set to (15,0) and (14,0), respectively. The radius r of the cross-section is assumed to be

$$r = r_0 + \delta r \sin n\theta, \ (n = 0, \pm 1, \pm 2 \cdots) \tag{12}$$

where r_0 is the radius of the undeformed SWCNTs and $\delta r / a$ is the amplitude of the deformation (Fig. 1). We have set $n=4$ and changed $\delta r / a$, where a=0.246 nm is the lattice constant of CNTs, from 0 to 2.34×10^{-2}. Our calculation of the radially corrugated CNTs are conducted by the four orbital whose Slater-Koster parameters are given in Table 1 (Papaconstantopoulos *et al.* 1998). 60 points of wave numbers are plotted to draw the band structure and one period is necessary and sufficient for draw the band structure, the atomic structure of which is given in Fig. 2. The period lengths of CNTs $L_{(n,m)}$ is given by (Ando 2005)

$$L_{(n,m)} = \frac{\sqrt{3}a\sqrt{n^2 + m^2 + nm}}{d_R} \tag{13}$$

where the set of n and m is integer and determines the chirality of CNTs. d_R is the greatest common divisor of $2m+n$ and $2n+m$. Therefore, the length of (15,0) and (14,0) CNT are

$$L_{(15,0)} = \frac{\sqrt{3} \times 0.246 \times 15}{15} \sim 0.426 \, [nm] \tag{14}$$

and

$$L_{(14,0)} = \frac{\sqrt{3} \times 0.246 \times 14}{14} \sim 0.426 \, [nm] \tag{15}$$

respectively. The number of atoms of CNTs $N_{(n,m)}$ is given by (Ando 2005)

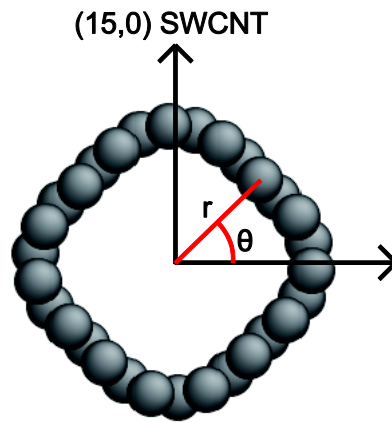$$N_{(n,m)} = \frac{4(n^2 + m^2 + nm)}{d_R} \tag{16}$$

(15,0) SWCNT

Fig. 1 Top view of the atomic configuration in the axial direction. The (15,0) zigzag SWCNT is radially corrugated with $\delta r / a = 2.34 \times 10^{-2}$ and $n = 4$
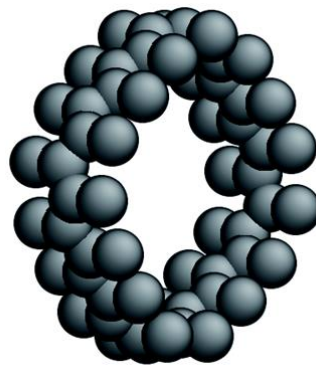

Fig. 2 One period of the radially corrugated atomic configuration of the (15,0) zigzag SWCNT; $\delta r / a = 2.34 \times 10^{-2}$ and $n = 4$
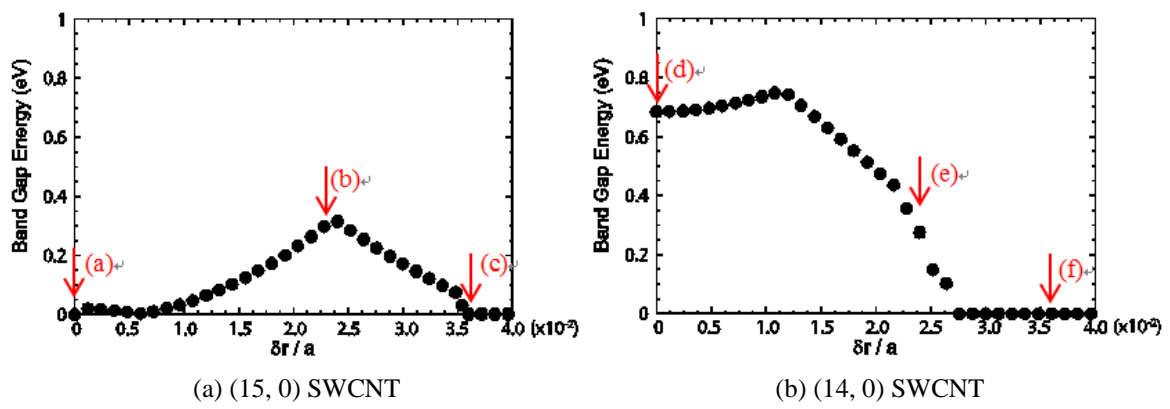

(a) (15, 0) SWCNT

(b) (14, 0) SWCNT

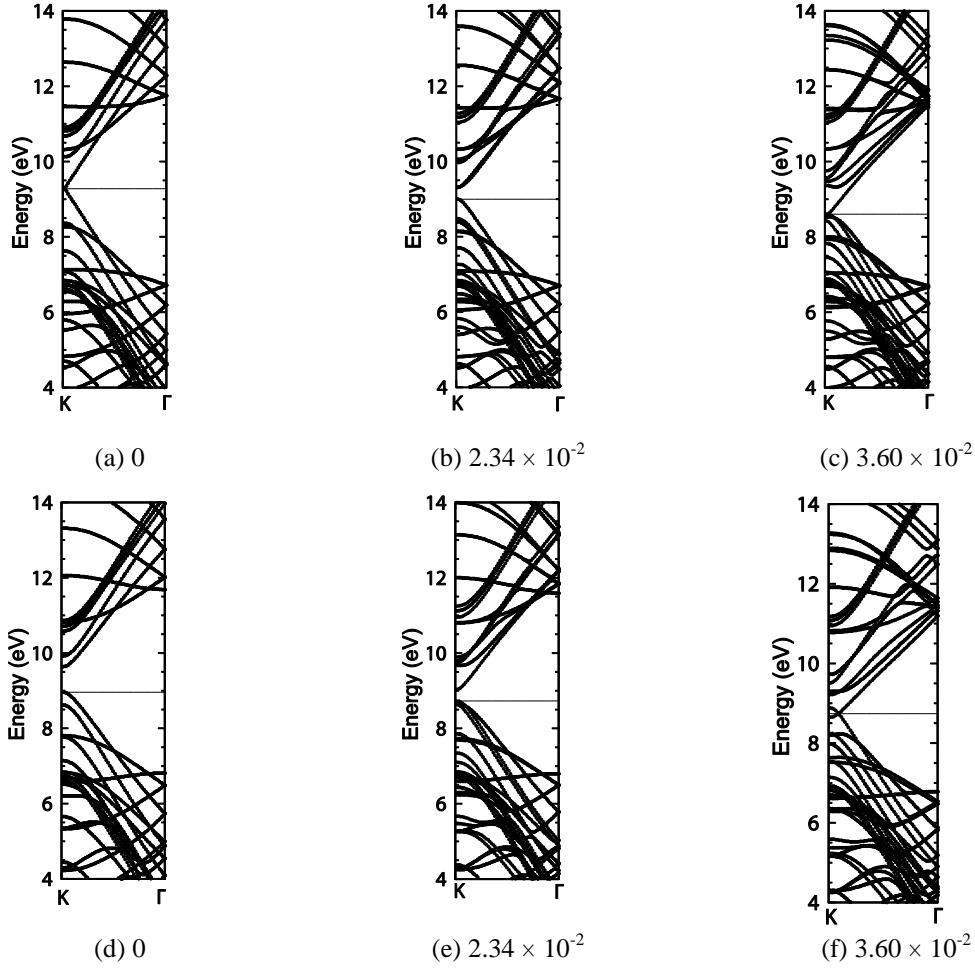Fig. 3 Change in band gap energy under radial corrugation

Fig. 4 Dispersion relation under radial corrugation in the case of the (a)-(c) (15,0), (d)-(f) (14,0) zigzag SWCNT. (15,0) SWCNT is the metallic material without any deformation, while (14,0) SWCNT is the semiconducting material without any deformation.

Therefore, $N_{(n,m)}$ of (15,0) and (14,0) CNT are

$$N_{(15,0)} = \frac{4 \times 15^2}{15} = 60 \tag{17}$$

and

$$N_{(14,0)} = \frac{4 \times 14^2}{14} = 56 \tag{18}$$

respectively. We note that $L_{(n,m)}$ and $N_{(n,m)}$ given in here are defined in the unit cell, and periodic boundary condition is imposed in the axial direction of CNTs. This means that CNTs have an

infinite length in the axial direction.

4. Results and discussion

Fig. 3 shows the band gap energy ΔE as a function of $\delta r / a$ in the case of a (15,0) zigzag SWCNT whose ΔE is zero at $\delta r / a = 0$, i.e., without any deformation, which means that the (15,0) zigzag SWCNT is in a metallic state as is well known. We found that ΔE increases with an increasing $\delta r / a$ and reaches the maximum value at $\delta r / a \approx 2.4 \times 10^{-2}$. Further increase in $\delta r / a$ causes a decrease in ΔE, and finally ΔE becomes zero. We should emphasize that these observations show the metal-semiconductor-metal transition induced by radial corrugation. The ΔE of the (14,0) zigzag SWCNT is finite at $\delta r / a = 0$, and this is a well-known characteristic of semiconducting CNTs. With an increasing $\delta r / a$, ΔE slightly increases to $\Delta E \approx 0.75$ eV when $\delta r / a$ is about 1.2×10^{-2}, and then, ΔE decreases to zero. This means that the (14,0) CNT under radial corrugation undergoes a semiconductor-metal transition. We note that anisotropic compression does not contribute to the increase in ΔE (Umeno *et al.* 2004, Umeno 2011). This means that anisotropic compression of the cross-section plays an essentially different role than the isotropic counterpart by hydrostatic pressure, although both the two fall into the category of radial deformation.

These transitions are attributable to the alternation of the band branch with regard to the highest occupied molecular orbital (HOMO) and lowest unoccupied molecular orbital (LUMO) shown in Fig. 4. Fig. 4 shows the electronic band structure for three different values of $\delta r / a$, which are set to (a) and (d) 0, (b) and (e) 2.34×10^{-2}, (c) and (f) 3.60×10^{-2}. The top three and bottom three panels show the band structure in the case of (15,0) and (14,0) zigzag SWCNTs, respectively. The band branch of the HOMO shifts to the higher energy region, and that of the next highest occupied molecular orbital (NHOMO) shifts to the lower energy region with an increasing $\delta r / a$. This situation explains the metal-to-semiconductor transition. These two branches cross, and the HOMO branch changes into the NHOMO branch, and vice versa, at some value of $\delta r / a$, as shown in Figs. 4 (b) and 4(e). The semiconductor to metal transition can be explained that several band overlaps further increase of $\delta r / a$ given in Figs. 4 (c) and 4(f). The same situation occurs for the LUMO and the next lowest unoccupied molecular orbital.

Radial corrugation is realized by the interaction between the SWCNTs and the elastic medium. Our model does not take this interaction into account, but simply corrugates the cross-sectional shape artificially according to Eq. (9). Therefore, a more realistic atomic configuration should be calculated by using, for example, a molecular dynamics simulation.

5. Conclusion

We numerically calculated the band gap energy of (15, 0) and (14, 0) SWCNTs under radial corrugation. The radial corrugation induced a metal-semiconductor-metal and a semiconductor-metal transition in the cases of the (15, 0) and (14, 0) SWCNTs, respectively. These findings can be understood by observing the dispersion relation, that is, the HOMO and LUMO band branches change with an increasing $\delta r / a$.

Acknowledgments

References

Aghaei A. and Dayal K. (2012), "Tension and twist of chiral nanotubes: torsional buckling, mechanical response and indicators of failure", *Model. Simul. Mater. Sci. Eng.,* **20**(8), 0850011-08500113.

Ando T (2005), "Theory of electronic states and transport in carbon nanotubes", *J. Phys. Soc. Jpn.,* **74**(3), 777-817.

Azevedo S., Rosas A., Machado M., Kaschny J.R. and Chacham H. (2013), "Effects of deformation on the electronic properties of B-C-N nanotubes", *J. Sol. Stat. Chem.,* **197**, 254-260.

Barboza A.P.M., Gomes A.P., Archanjo B.S., Araujo P.T., Jorio A. and Ferlauto A.S. (2008), "Deformation induced semiconductor-metal transition in single wall carbon nanotubes probed by electronic force microscopy", *Phys. Rev. Lett.,* **100**(25), 2568041-2568044.

Chen W., Andreev A.V., Tsvelik A.M. and Orgad D. (2008), "Twist Instability in strongly correlated carbon nanotubes", *Phys. Rev. Lett.,* **101**(24), 2468021-246804.

Chesnokov S.A., Nalimova V.A., Rinzler A.G., Smalley R.E. and Fischer J.E. (1999), "Mechanical energy storage in carbon nanotube springs", *Phys. Rev. Lett.,* **82**(2), 343-346.

Choudhary S. and Qureshi S. (2012), "Theoretical study on effect of radial and axial deformation on electron transport properties in a semiconducting SiC nanotube", *Bull. Mater. Sci.,* **35**(5), 713-718.

Faria B., Silvestre N. and Canongia Lopes J.N. (2012), "Torsion-twisting dependent kinematics of chiral CNTs", *Compos. Sci. Tech.*, **74**(24), 211-220.

Faria B., Silvestre N. and Canongia Lopes J.N. (2013), "Induced anisotropy of chiral carbon nanotubes under combined tension-twisting", *Mech. Mater.*, **58**, 97-109.

Farshidianfar A. and Soltani P. (2012), "Nonlinear flow-induced vibration of a SWCNT with a geometrical imperfection", *Comp. Mater. Sci.,* **53**(1), 105-116.

He Z., Ke X., Bais S. and Tendeloo G.V. (2012), "Direct evidence for the existence of multi-walled carbon nanotubes with hexagonal cross-sections", *Carbon*, **50**(7), 2524-2529.

Huang X., Liang W. and Zhang S. (2011), "Radial corrugations of multi-walled carbon nanotubes driven by inter-wall nonbonding interactions", *Nanoscale Res. Lett.,* **6**, 531-536.

Ishii H., Kataura H., Shiozawa H. and Yoshioka H. (2003), "Gate-induced crossover from unconventional metals to Fermi liquids in multiwalled carbon nanotubes", *Nature,* **426**(6966), 540-544.

Kanbara T., Iwasa T., Tsukagoshi K., Aoyagi Y. and Iwasa Y. (2004), "Gate-induced crossover from unconventional metals to Fermi liquids in multiwalled carbon nanotubes", *Appl. Phys. Lett.,* **85**(26), 6404-6406.

Ke C.-H., Pugno N., Peng B. and Espinosa H.D. (2006), "Experiments and modeling of carbon nanotube-based NEMS", *J. Mech. Phys. Sol.,* **53**(6), 1314-1333.

Li C. and Chou T.W. (2003), "A structural mechanics approach for the analysis of carbon nanotubes", Int. J. Solids Struct., **40**(10), 2487-2499.

Lordi V. and Yao N. (1998), "Radial compression and controlled cutting of carbon nanotubes", *J. Chem. Phys.,* **109**(6), 2509-2512.

Lu W., Chou T-W. and Kim B-S. (2011), "Radial deformation and its related energy variations of single-walled carbon nanotubes", *Phys. Rev. B*, **83**(13), 1341131-1341138.

Mehl M.J. and Papaconstantpoulos D.A. (1996), "Applications of a tight-binding total-energy method for transition and noble metals: Elastic constants, vacancies, and surfaces of monatomic metals", *Phys. Rev.*

B, **54**(7), 4519-4530.

Nishidate K. and Hasegawa M. (2008), "Universal band gap modulation in semiconductor single-walled carbon nanotubes", *Phys. Rev. B,* **78**(19), 1954031-1954036.

Ono S. and Shima H. (2009), "Tuning the electrical resistivity of semiconductor thin films by nanoscale corrugation", *Phys. Rev. B*, **79**(23), 2354071-2354076.

Pantano A., Campanella D., Montinaro N. and Cerniglia D. (2013), "Electronic properties of carbon nanotubes under torsion", *Appl. Phys. A,* **110**(1), 77-85.

Papaconstantopoulos D.A., Mehl M.J., Erwin S.C. and Pederson M.R. (1998), "Tight-binding Hamiltonians for carbon and silicon", *MRS Symp. Proc.,* **491**, 221-224.

Poklonski N.A., Ratkevich S.V., Vyrko S.A., Kislyakov E.F., Bubel' O.N., Popov A.M., Lozovik Y.E., Hieu N.N. and Viet N.A. (2012), "Structural phase transition and band gap of uniaxially deformed (6,0) carbon nanotube", *Chem. Phys. Lett.,* **545**, 71-77.

Reich S., Thomsen C. and Ordejon P. (2002), "Elastic properties of carbon nanotubes under hydrostatic pressure", *Phys. Rev. B*, **65**(15), 153407.

Ren Y., Chen K.-Q., Wan Q., Zou B.S. and Zhang Y. (2009), "Transitions between semiconductor and metal induced by mixed deformation in carbon nanotube devices", *Appl. Phys. Lett.,* **94**(18), 1835061-1835063.

Shen W., Jiang, B., Han B.S. and Xie S.S. (2000), "Investigation of the radial compression of carbon nanotubes with a scanning probe microscope", *Phys. Rev. Lett.*, **84**(16), 3634-3637.

Shima H., Ghosh S., Arroyo M., Iiboshi K. and Sato M. (2012), "Thin-shell theory based analysis of radially pressurized multiwall carbon nanotubes", *Comp. Mater. Sci.,* **52**(1), 90-94.

Shima H. and Sato M. (2008), "Multiple radial corrugations in multiwalled carbon nanotubes under pressure", *Nanotechnology,* **19**(49), 495705:1-195705:8.

Shima H. and Sato M. (2009), "Pressure-induced structural transitions in multi-walled carbon nanotubes", *Phys. Stat. Sol. A,* **206**(10), 2228-2233.

Shima H., Sato M., Iiboshi K., Ghosh S. and Arroyo M. (2010), "Diverse corrugation pattern in radially shrinking carbon nanotubes", *Phys. Rev. B,* **82**(8), 0854011-0854017

Shima H., Yoshioka H. and Onoe J. (2009), "Geometry-driven shift in the Tomonaga-Luttinger exponent of deformed cylinders" *Phys. Rev. B*, **79**(20), 2014011-2014014.

Silvestre N. (2012), "On the accuracy of shell models for torsional buckling of carbon nanotubes", *Eur. J. Mech. A/Solids,* **32**, 103-108.

Silvestre N., Faria B. and Duarte A. (2012), "Multilevel approach for the local nanobuckling analysis of CNT-based composites", *Coupled Systems Mech.,* **1**(3), 269-283.

Tang D.S., Bao Z.X., Wang L.J., Chen L.C., Sun L.F., Liu Z.Q., Zhou W.Y. and Xie S.S. (2000), "The electrical behavior of carbon nanotubes under high pressure", *J. Phys. Chem. Solids*, **61**(7), 1175-1178.

Tang J., Qin L.C., Sasaki T., Yudasaka M., Matsushita A. and Iijima S. (2000), "Compressibility and polygonization of single-walled carbon nanotubes under hydrostatic pressure", *Phys. Rev. Lett.,* **85**(9), 1887-1889.

Tang J., Qin L.C., Sasaki T., Yudasaka M., Matsushita A. and Iijima S. (2002), "Revealing properties of single-walled carbon nanotubes under high pressure", *J. Phys.: Condens. Matt.*, **14**(44), 10575-10578.

Umeno Y. (2011), "Tight-binding calculation of deformation and band gap of single-walled carbon nanotubes under axial tension and radial compression", *Proc. Eng.,* **14**(24), 2386-2393

Umeno Y., Kitamura T. and Kushima A. (2004a), "Theoretical analysis on electronic properties of zigzag-type single-walled carbon nanotubes under radial deformation", *Comp. Mater. Sci.,* **30**(3-4), 283-287.

Umeno Y., Kitamura T. and Kushima A. (2004b), "Metallic-semiconducting transition of single-walled carbon nanotubes under high axial strain", *Comp. Mater. Sci.,* **31**(1-2), 33-41.

Wong J.H., Wu B.R. and Lin M.F. (2012), "Strain Effect on the Electronic Properties of Single Layer and Bilayer Graphene" *J. Phys. Chem. C*, **116**(14), 8271-8277.

Yu M.F., Kowalewski T. and Ruoff R.S. (2000), "Investigation of the radial deformability of individual carbon nanotubes under controlled indentation force", *Phys. Rev. Lett.*, **85**(7), 1456-1459.